Journal of the Taiwan Institute of Chemical Engineers 000 (2015) 1–7

Contents lists available at ScienceDirect

Journal of the Taiwan Institute of Chemical Engineers

journal homepage: www.elsevier.com/locate/jtice

Novel Keggin-type $H_4PVMo_{11}O_{40}$-based ionic liquid catalysts for *n*-caprylic acid esterification

Xiaoxiang Han[a,*], Keke Chen[a], Huan Du[a], Xiu-Juan Tang[b], Chin-Te Hung[c], Kai-Chen Lin[c,d], Shang-Bin Liu[c,d,**]

[a] Department of Applied Chemistry, Zhejiang Gongshang University, Hangzhou 310018, China
[b] College of Environmental Science and Engineering, Zhejiang Gongshang University, Hangzhou 310018, China
[c] Institute of Atom and Molecular Sciences, Academic Sinica, Taipei 10617, Taiwan
[d] Department of Chemistry, National Taiwan Normal University, Taipei 11677, Taiwan

ARTICLE INFO

Article history:
Received 5 March 2015
Revised 30 June 2015
Accepted 2 July 2015
Available online xxx

Keywords:
Heteropolyacid-based ionic liquid
Esterification
Acidity
Methyl caprylate
Response surface methodology

ABSTRACT

A series of new Keggin-type heteropolyacid (HPA)-based ionic liquid catalysts were synthesized from molybdovanadophosphoric acid ($H_4PVMo_{11}O_{40}$) and propane sulfonated ionic liquid (MIM-PS). The physicochemical properties of these inorganic–organic composite catalysts were characterized by various techniques such as FT-IR, TGA, high-resolution ^1H and ^{13}C NMR, and solid-state ^{31}P MAS NMR. Their catalytic performances were evaluated for esterification of *n*-caprylic acid to methyl caprylate, among them, the $[MIM\text{-}PSH]_{2.0}H_{2.0}PVMo_{11}O_{40}$ catalyst revealed an optimal reaction activity. Moreover, an experimental design was exploited *via* response surface methodology (RSM) on the basis of the Box–Behnken design (BBD). Accordingly, a maximum methyl caprylate yield of 95.6% was obtained over the $[MIM\text{-}PSH]_{2.0}H_{2.0}PVMo_{11}O_{40}$ catalyst under the optimal conditions: catalyst to *n*-caprylic acid molar ratio 0.52 mol%, methanol/acid molar ratio of 7, reaction time 3.0 h, and temperature 363 K. These results were in conformity with those predicted by a mathematical model. A desirable durability may also be inferred for the reported catalyst; no considerable change in catalyst performance was observed during six successive cyclic operations. The improved acidic strength and lower molecular transport resistance of the catalysts were accounted for the superior catalytic performance and durability observed.

© 2015 Taiwan Institute of Chemical Engineers. Published by Elsevier B.V. All rights reserved.

1. Introduction

Carboxylic esters have attracted widespread attentions for their extensive applications in food, cosmetics, biodiesel, pharmaceutical, chemical industry and so on [1]. Conventionally, they are synthesized through esterification over mineral acid catalysts, such as sulfuric [2], *p*-toluene sulfonic [3], and phosphoric acid [4]. However, these homogeneous catalysts are hampered by several inherent drawbacks, such as equipment corrosion, environmental pollution, side reactions, difficulty in catalyst recovery and reuse. Thus, considerable efforts have been made on the development of effective and eco-friendly catalysts such as heteropolyacids (HPAs) [5,6], molecular sieves [7,8], solid super acids [9], zeolites [10], resins [11], and enzymes [12] for esterification. Among which, HPAs have shown excellent catalytic activity and selectivity owing to their ultra-strong acidic strength and unique pseudoliquid characteristics [5]. To circumvent their low specific surface area and inconvenient separation [13], researchers have attempted to support heteropolyacids on appropriate carriers, *e.g.*, activated carbons [14], Al_2O_3 [15], SnO_2 [16], ZrO_2 [17], zeolites [18], resins [19], and clays [20], in order to modify their solubility and the distribution of acid sites on catalyst surface.

On the other hand, ionic liquids (ILs) have been widely applied as new eco-friendly catalysts owing to their negligible volatility, high thermal stability, excellent solubility, tunable properties, easy recovery, and reusability [21,22]. While some reports on catalytic performance during esterification reaction over pure IL catalysts are available in the literature [23], herein, it was exploited as a carrier for loading solid superacids, namely HPAs. In this work, a series of such inorganic–organic (TPA-IL) catalysts were synthesized by incorporating varied amounts of molybdovanadophosphoric acid ($H_4PVMo_{11}O_{40}$) with 3-(1-methylimidazolium-3-yl) propane-1-sulfonate ionic liquid (MIM-PS) to form various $[MIM\text{-}PSH]_xH_{4-x}PVMo_{11}O_{40}$ (x = 1.0–4.0) composite salts. The physicochemical properties of the novel composite catalysts so prepared were characterized by a variety of different techniques such as Fourier-transform infrared (FT-IR), thermogravimetric analysis (TGA),

* Corresponding author. Tel.: +86 571 28008975.
** Corresponding author at: Institute of Atom and Molecular Sciences, Academic Sinica, Taipei 10617, Taiwan. Tel.: +886 2 23668230.
E-mail addresses: hxx74@126.com (X. Han), sbliu@sinica.edu.tw (S.-B. Liu).

http://dx.doi.org/10.1016/j.jtice.2015.07.005
1876-1070/© 2015 Taiwan Institute of Chemical Engineers. Published by Elsevier B.V. All rights reserved.

and high-resolution ^{1}H and ^{13}C nuclear magnetic resonance (NMR). Their acidic properties were investigated by solid-state ^{31}P magic-angle-spinning (MAS) NMR using trimethylphosphine oxide (TMPO) as the probe molecule. The catalytic activities of these catalysts for esterification of *n*-caprylic acid with methanol were also examined. Relevant reaction process and product optimizations were accomplished by means of a factorial experimental design and response surface methodology (RSM).

2. Experimental

2.1. Catalyst preparation

The molybdovanadophosphoric acid ($H_4PVMo_{11}O_{40}$) was prepared by stepwise acidification following a reported procedure [24]. In brief, a mixture of disodium hydrogen phosphate ($Na_2HPO_4 \cdot 12H_2O$; 0.01 mol) and sodium molybdate ($Na_2MoO_4 \cdot 2H_2O$; 0.11 mol) was dissolved into 80 mL distilled water and stirred at reflux temperature (373 K) for 0.5 h. Then, a proper amount of ammonium metavanadate (NH_4VO_3; 0.01 mol) was slowly added to the mixture solution under continuous stirring for additional 0.5 h while adjusting pH to 2.0–2.5 by sulfuric acid. After cooling to the room temperature (298 K), the mixture was washed with ethyl ether in sulfuric acid medium, followed by the calcination treatment in air (523 K; 2.0 h) to obtained the orange red powder of $H_4PVMo_{11}O_{40}$ as the final HPA product. Further analysis by inductively coupled plasma atomic emission spectroscopy (ICP-AES; Euro EA 3000) technique revealed that the product contained elements of P (1.52%), Mo (51.62%), and V (2.47%), which are in good agreement with the calculated values of 1.54%, 52.38%, and 2.53%, respectively.

The zwitterion 3-(1-methylimidazolium-3-yl) propane-1-sulfonate ionic liquid (MIM-PS) was also prepared following a known procedure [25]. The composite catalysts were prepared by adding MIM-PS to an aqueous solution of $H_4PVMo_{11}O_{40}$ under varied molar ratios. The mixture was first heated at 363 K for 24 h, followed by solvent removal with rotary evaporation, and then washed with ethyl ether. The final products of $[MIM\text{-}PSH]_xH_{4-x}PVMo_{11}O_{40}$ composite catalysts were obtained after drying in a vacuum oven, where $x = 1.0–4.0$ represents the molar ratio of MIM-PS to $H_4PVMo_{11}O_{40}$.

2.2. Characterization method

FT-IR spectra of various HPA-based IL catalysts and their precursors, namely $H_4PVMo_{11}O_{40}$ and MIM-PS, were recorded on a Bruker IFS-28 spectrometer over the 4000–400 cm^{-1} region using KBr as the reference. Thermogravimetric and differential thermogravimetric (TG–DTG) analyses of various samples were performed on a TG-209 (NETZSCH) apparatus. Samples were heated from room temperature to 873 K at a heating rate of 10 K/min under the protection of nitrogen. High-resolution ^{1}H and ^{13}C NMR spectra of assorted samples (in D_2O) were recorded on a Bruker AV500 spectrometer at Larmor frequencies of 500.13 and 125.76 MHz, respectively. On the other hand, solid-state ^{31}P MAS NMR studies were performed on a Bruker-Biospin AVANCE III 500 spectrometer (at Larmor frequency of 202.46 MHz) using a 4-mm double-resonance MAS probehead operating at a spinning rate of 12 kHz. All ^{31}P spectra were acquired using a single-pulse sequence with an excitation pulse of 1.5 μs (*ca.* $\pi/6$) and a recycle delay of 10 s. The ^{31}P NMR chemical shifts ($\delta^{31}P$) were referenced to 85% H_3PO_4 aqueous solution.

Solid-state ^{31}P MAS NMR of adsorbed trimethylphosphine oxide (TMPO) has been proven to be a power tool for probing the acidic properties of acid catalysts [26–28]. Prior to the adsorption of TMPO probe molecule, catalyst was first dehydrated at 423 K for 24 h under vacuum ($< 10^{-5}$ Torr). Subsequently, a known amount of TMPO dissolved in CH_2Cl_2 solution was introduced into a vessel containing the dehydrated sample. This procedure was carried out in a glove box under N_2 environment. The sealed sample vessel was then connected to a vacuum manifold, followed by the removal of CH_2Cl_2 solvent at 323 K. Then, the sample was further subjected to a thermal treatment at 393 K for at least 24 h to ensure a uniform adsorption of the adsorbate probe molecules in the substrate. Finally, the TMPO-loaded sample was transferred into a MAS rotor in a N_2 glove box, and then sealed by a gas-tight Kel-F cap.

2.3. Catalytic reaction

The catalytic activities of the various $[MIM\text{-}PSH]_xH_{4-x}PVMo_{11}O_{40}$ ($x = 1.0–4.0$) catalysts were examined by esterification reaction. Typically, *n*-caprylic acid (0.1 mol) and known amounts of methanol and the test catalyst were charged into a three-necked flask equipped with a mechanical stirrer, a reflux condenser, and a drop funnel containing molecular sieves (3 Å). Prior to each run, the reaction mixture was first pre-heated at a fixed temperature for a desired time before cooling to the room temperature. Owing to the self-separation characteristics of the reaction system, the precipitated catalyst may easily be separated after the esterification reaction. The catalyst may readily be recovered and ready for recycle use after simple filtering and washing (with diethyl ether) procedures. Quantitative analysis of the products was performed by a gas chromatograph (GC; Agilent 6890N) equipped with a FID detector and HP-5 capillary column. Reactants and products were identified by comparing with authentic samples using methyl laurate as an internal standard.

2.4. Design of experiments and response surface methodology

The response surface methodology (RSM) was used to optimize the reaction process and product yield during the esterification reaction [29,30]. A Box–Behnken design was applied to study the effects of three process variables (catalyst to *n*-caprylic acid ratio, methanol to *n*-caprylic acid ratio and reaction time) on esterification of *n*-caprylic acid. A total of 17 runs were required, which included 12 factorial points and 5 center points.

A model equation based on the quadratic polynomial given by RSM was used to reveal interactive effects between experimental variables, to optimize the reaction process, and to predict the yield of the product (*i.e.*, methyl caprylate). The model equation may be expressed as:

$$Y = \beta_0 + \sum_{i=1}^{3} \beta_i x_i + \sum_{i=1}^{3} \beta_{ii} x_i^2 + \sum_{i<j}^{3} \beta_{ij} x_i x_j \quad (1)$$

where Y was the predicted response, x_i and x_j were the coded levels of the independent variables, β_0 was the center point of the system, β_i, β_{ii}, β_{ij} were the linear terms, the squared terms for the variable *i*, and the interaction terms between variables *i* and *j*, respectively. The Design-Expert 6.0.5 software (Stat-Ease, USA) was used to analyse the experimental data, to perform analysis of variance (ANOVA), and to evaluate the regression equation. Accordingly, the fitted polynomial equation may further be expressed in terms of response surface and contour plots to facilitate visualization of the correlations between the response and experimental variables at various coded levels, and to infer optimized process conditions.

3. Results and discussions

3.1. Catalyst properties

The FT-IR spectra of various heteropolyacid-based ionic liquids $[MIM\text{-}PSH]_xH_{4-x}PVMo_{11}O_{40}$ ($x = 1.0–4.0$) catalysts and their precursors, namely $H_4PVMo_{11}O_{40}$ and MIM-PS, are displayed in Fig. 1. For

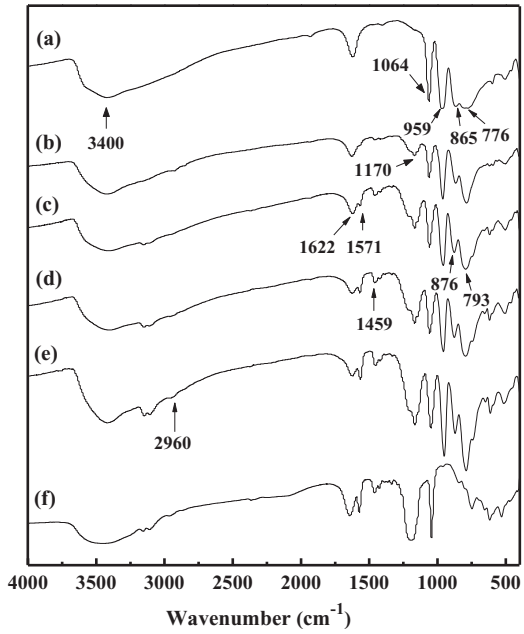

Fig. 1. FT-IR spectra of heteropolyacid-based ionic liquid catalysts and relevant precursors: (a) $H_4PVMo_{11}O_{40}$, (b) $[MIM\text{-}PSH]_{1.0}H_{3.0}PVMo_{11}O_{40}$, (c) $[MIM\text{-}PSH]_{2.0}H_{2.0}PVMo_{11}O_{40}$, (d) $[MIM\text{-}PSH]_{3.0}H_{1.0}PVMo_{11}O_{40}$, (e) $[MIM\text{-}PSH]_{4.0}PVMo_{11}O_{40}$, and (f) MIM-PS.

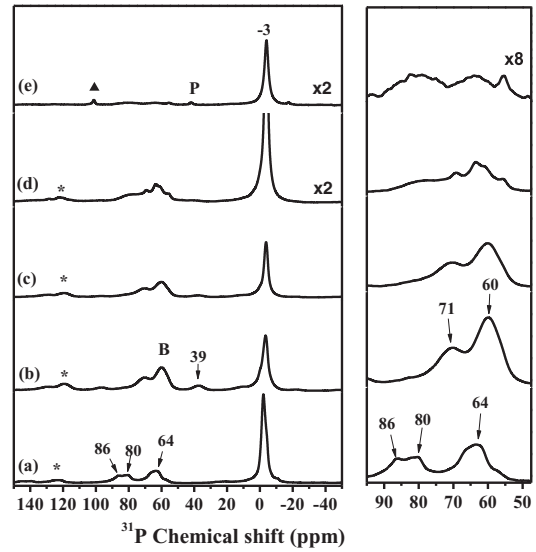

Fig. 2. ^{31}P MAS NMR spectra of TMPO adsorbed on (a) pristine $H_4PVMo_{11}O_{40}$ and various $[MIM\text{-}PSH]_xH_{4-x}PVMo_{11}O_{40}$ with (b) $x = 1.0$, (c) $x = 2.0$, (d) $x = 3.0$, and (e) $x = 4.0$ catalysts recorded with a spinning frequency of 12 kHz and a relative TMPO loading of (a) : (b) : (c) : (d) : (e) = 4.0 : 3.0 : 2.0 : 1.0 : 1.0. The asterisks (∗) and solid triangle (▲) represent spinning sidebands arising from the primary peak corresponding to Brønsted acidity (B) and physisorbed TMPO (P), respectively. Right: blow-up spectra over the peak region associated with Brønsted acidity.

the pristine $H_4PVMo_{11}O_{40}$, four distinctive characteristic bands corresponding to different bridging-oxygen environments of the Keggin structure were observed, *viz.* asymmetric stretching vibration of P–O_a (1050–1070 cm^{-1}), terminal Mo=O_d (950–970 cm^{-1}), corner-sharing Mo–O_b–Mo (860–880 cm^{-1}), and edge-sharing Mo–O_c–Mo (770–800 cm^{-1}) [31], in spite of the slight variations in intensity and frequency of the bands in various samples. Vibrational bands responsible for V–O appeared to be overlapped with the above peaks. In addition to the aforementioned bands, the IR spectra observed for various $[MIM\text{-}PSH]_xH_{4-x}PVMo_{11}O_{40}$ (x = 1.0–4.0) composite catalysts also reveal peaks around at 3400, 1622, and 1571 cm^{-1}, which may be attributed to stretching vibrations of O–H [32], C=C, and C=N of the imidazole ring [33,34], respectively. Whereas the absorption bound at 1170 cm^{-1} may be ascribed due to S=O stretching vibration [35]. In addition, the peaks at 2960 and 1459 cm^{-1} should be associated with the C–H stretching and deformation vibrations. The appearance of these bands together with the increases in their peak intensities with increasing x value, indicate the progressive anchoring of the MIM-PS IL onto the HPA. The above observations therefore verify the successful linkage between the sulfonate functionalized organic cations and the inorganic polyanions ($PVMo_{11}O_{40}^{4-}$).

TGA–DTG analysis was utilized to explore the thermal stability of various samples. Each sample was heated from room temperature to 873 K under the protection of nitrogen. As depicted in Fig. S1a of the Supplementary materials, the parent MIM-PS IL showed only a weight-loss peak centering at *ca.* 642 K [36,37]. Since the $[MIM\text{-}PSH]_xH_{4-x}PVMo_{11}O_{40}$ (x = 1.0–4.0) catalysts exhibit similar thermal properties, hence, similar TGA–DTG profiles were observed. Herein, we focus on results obtained from the $[MIM\text{-}PSH]_{2.0}H_{2.0}PVMo_{11}O_{40}$ sample. As shown in Fig. S1b (Supplementary materials), the DTG curve observed for the $[MIM\text{-}PSH]_{2.0}H_{2.0}PVMo_{11}O_{40}$ sample showed multiple weight-loss peaks. Among them, the peak centering at 316, 443, and 834 K should be arising from the evaporation of surface-bounded water, elimination of crystal water, and weight-loss of constituent water and decomposition of the Keggin unit anions, respectively. Note that similar desorption peaks were observed for the pristine $H_4PVMo_{11}O_{40}$ (Fig. S1c; Supplementary materials). Moreover, the peak occurred at 625 K may be attributed to the decomposition of organic moieties of $[MIM\text{-}PSH]_{2.0}H_{2.0}PVMo_{11}O_{40}$, namely from the weight-loss of MIMPS (see Fig. S1a; Supplementary materials). The above results therefore indicated that the MIM-PS IL was successfully linked to the Keggin $PVMo_{11}O_{40}^{4-}$ polyanions and the composite catalysts remained stable within the temperature range employed in the reaction system.

The structural integrity of the $[MIM\text{-}PSH]_xH_{4-x}PVMo_{11}O_{40}$ (x = 1.0–4.0) composite catalysts was further verified by ^1H and ^{13}C NMR. Since all composite catalysts exhibited similar ^1H and ^{13}C NMR spectra (not shown), as expected, here, only the spectral data observed for the $[MIM\text{-}PSH]_{2.0}H_{2.0}PVMo_{11}O_{40}$ sample were listed below: ^1H NMR (500 MHz, D_2O, TMS): δ 2.206 (m, 2H), 2.812 (t, 2H), 3.822 (s, 3H), 4.290 (t, 2H), 7.360 (d, 1H), 7.428 (d, 1H), 8.624 (s, 1H) ppm; ^{13}C NMR (500 MHz, D_2O): δ 25.11, 35.75, 47.25, 47.79, 122.25, 123.86, 135.98 ppm. Additional study by field-emission scanning electron microscopy (FE-SEM) revealed a similar morphology for various composite catalysts; the homogeneously distributed catalyst particles are mostly elliptical in shape with a typical size of *ca.* 5–10 μm (see Fig. S2; Supplementary materials).

In addition, the acidic properties of various samples were studied by solid-state ^{31}P MAS NMR of adsorbed trimethylphosphine oxide (TMPO); which was proven to be a powerful technique for acidity characterization of solid acid catalysts [26– 28,38,39]. The base TMPO probe molecule tended to interact with the Brønsted acidic protons to form $TMPOH^+$ adducts, whose ^{31}P NMR chemical shift ($\delta^{31}P$) was directly proportional to the acidic strength of the catalyst [38,39]. The ^{31}P MAS NMR spectra of TMPO adsorbed on the pristine $H_4PVMo_{11}O_{40}$ and various $[MIM\text{-}PSH]_xH_{4-x}PVMo_{11}O_{40}$ (x = 1.0–4.0) catalysts were shown in Fig. 2. The sharp ^{31}P resonance located at −3 ppm may be unambiguously attributed to the signal arising from the Keggin polyanions ($PVMo_{11}O_{40}{}^{4-}$) of the heteropolyacid acid [40,41]. Moreover, the peak at *ca.* 39 ± 2 ppm is ascribed due to ^{31}P signal of physisorbed TMPO, whereas peaks with $\delta^{31}P$ in the region of 53–90 ppm were assigned due to TMPO adsorbed on Brønsted acid sites with differing acidic strengths [26– 28,38,39]. Since a chemical shift value of 86 ± 2 ppm has been inferred for the threshold of superacidity based on the ^{31}P-TMPO approach [38,39]. The presence of the ^{31}P signal with $\delta^{31}P$ = 86 ppm in Fig. 2a revealed that the pristine $H_4PVMo_{11}O_{40}$ catalyst indeed possesses superacidity, whereas

Table 1
Catalytic performances of various catalysts during esterification of *n*-caprylic acid with methanol[a].

Catalyst	Methyl caprylate yield (%)
MIM-PS	49.4
$H_4PVMo_{11}O_{40}$	86.4
$[MIM\text{-}PSH]_{1.0}H_{3.0}PVMo_{11}O_{40}$	89.1
$[MIM\text{-}PSH]_{2.0}H_{2.0}PVMo_{11}O_{40}$	91.5
$[MIM\text{-}PSH]_{3.0}H_{1.0}PVMo_{11}O_{40}$	71.7
$[MIM\text{-}PSH]_{4.0}PVMo_{11}O_{40}$	62.7

[a] Reaction conditions: catalyst weight 0.86 g; methanol : *n*-caprylic acid = 5 : 1 (mol : mol), reaction time 3.0 h, and temperature 363 K.

peaks at *ca.* 80 and 64 ppm may be due to distorted $TMPOH^+$ and $(TMPO)_2H^+$ adducts, respectively. The $\delta^{31}P$ values observed for the latter two peaks were in close resemblance with that observed for typical zeolitic catalysts [26].

However, since each $[MIM\text{-}PSH]_xH_{4-x}PVMo_{11}O_{40}$ catalyst contains varied amount of Brønsted acidic protons varying from $x = 1.0$–4.0, to avoid interference of ^{31}P NMR signals in the Brønsted acid region ($\delta^{31}P \sim 53$–90 ppm region) arising from physisorbed TMPO, the spectra shown in Fig. 2 was acquired with varied TMPO loading. A relative TMPO loading of 4.0 : 3.0 : 2.0 : 1.0 : 1.0 was introduced to $H_4PVMo_{11}O_{40}$, $[MIM\text{-}PSH]H_{3.0}PVMo_{11}O_{40}$, $[MIM\text{-}PSH]_{2.0}H_{2.0}PVMo_{11}O_{40}$, $[MIM\text{-}PSH]_{3.0}HPVMo_{11}O_{40}$ and $[MIM\text{-}PSH]_{4.0}PVMo_{11}O_{40}$ catalysts, respectively. In this context, the ^{31}P MAS NMR results can only afford qualitative information rather than quantitative data. Nevertheless, it is anticipated that the amount of available Brønsted acidic (H^+) sites (*i.e.*, acid concentration) in the above five samples should decrease with increasing proportional value of *x* (4 : 3 : 2 : 1 : trace (<<1). Moreover, upon a progressive incorporation of MIM-PS IL onto the pristine $H_4PVMo_{11}O_{40}$, notable decreases in $\delta^{31}P$ of NMR resonances responsible for TMPO adsorbed on Brønsted acid sites in various $[MIM\text{-}PSH]_xH_{4-x}PVMo_{11}O_{40}$ ($x = 1.0$–4.0) catalysts were observed (Fig. 2b–e), revealing a consistent decrease in acidic strength with increasing *x* value.

3.2. Esterification reaction

For acid-catalyzed reactions such as esterification reaction, the order of acidity was normally consistent with the order of activity in a catalyst system. The catalytic performances during esterification of *n*-caprylic acid with methanol over various catalysts examined herein were depicted in Table 1. In this context, the surface area of the catalyst appears irrelevant to the observed catalytic activity. The main drawbacks for using HPAs as catalysts are the fact that they have low surface areas (typically < 10 m^2/g) and the difficulty in product separation. The pristine $H_4PVMo_{11}O_{40}$ sample used herein was determined to possess a rather low surface area (7.1 m^2/g). Upon anchoring the MIM-PS ionic liquid, only marginal increase in surface area was observed for the composite catalysts. For example, the surface areas of 7.8 and 7.5 m^2/g were determined for the $[MIM\text{-}PSH]_{2.0}H_{2.0}PVMo_{11}O_{40}$ and $[MIM\text{-}PSH]_{4.0}PVMo_{11}O_{40}$ catalysts, respectively. On the other hand, their excellent solubility in water and polar solvents as well as the unique pseudoliquid characteristics were favorable for the excellent catalytic activity observed [5,36,40–43].

One of the advantages of these newly reported $[MIM\text{-}PSH]_xH_{4-x}PVMo_{11}O_{40}$ ($x = 1.0$–4.0) catalysts was that they could be utilized in both homogeneous and heterogeneous catalytic systems. It is noteworthy that while these catalysts are highly soluble in water and strong polar solvents, they are insoluble in esters. Indeed, the system was strictly homogeneous during the initial stage of the reaction due to complete dissolution of the catalyst in the presence of methanol and water. However, as the reaction proceeded, the reaction system gradually became turbid milky in the presence of esters as products. Upon completion of the esterification reaction, the high yield of esters provoked the occurrence of spontaneous self-separation, leading to biphasic layers consisting of segregated products and colloidal catalyst. Upon withdrawing the products in the upper layer, the precipitated catalyst could then be recycled after simple filtering and washing treatments. Similar behaviors were also found in other HPA-IL systems [29,37,43].

As shown in Table 1, the reaction carried out over the parent MIM-PS IL resulted in an inferior methyl caprylate yield of only 49.4%. Clearly, the parent sulfonated MIM-PS ionic liquid indeed possessed some acidity, which was capable of catalyzing the esterification reaction [37,42]. In comparison, the pristine $H_4PVMo_{11}O_{40}$ catalyst, which possessed an ultra-strong acidity, showed an improved product yield (86.4%). From the perspective of process operation, although the MIM-PS and $H_4PVMo_{11}O_{40}$ catalysts both are soluble in methanol, they provoke tedious process in product separation, hence, unfavorable for catalyst recycling. Upon progressive incorporation of MIM-PS IL onto the $H_4PVMo_{11}O_{40}$, the methyl caprylate yield observed for the $[MIM\text{-}PSH]_xH_{4-x}PVMo_{11}O_{40}$ ($x = 1.0$–4.0) catalysts gradually increased at first, then, decreasing with increasing *x* value. The incorporation of MIM-PS IL onto the HPA catalyst may also be beneficial to the separation of $H_4PVMo_{11}O_{40}$ to favor mass transfer of reactants and products. Among various composite catalysts examined, the $[MIM\text{-}PSH]_{2.0}H_{2.0}PVMo_{11}O_{40}$ sample exhibited the best catalytic activity with a methyl caprylate yield of 91.5%. In this context, it is indicative that ultra-strong acidity may be unfavorable for the esterification reaction. This may be attributed to the occurrence of the acid-catalyzed reverse reactions that, in turn, tends to spoil the product yield due to hydrolysis of methyl caprylate to *n*-caprylic acid and methanol. Further increase in MIM-PS loading ($x > 2.0$) resulted in a gradual decrease in product yield. This can be ascribed due to the weaker acidic strengths and lower acid concentration of the catalysts, which tend to enhance spatial hindrance in the reaction system, hence, leading to ineffective accessibility of reactants to the Brønsted acid protons (H^+).

3.3. Effects of experimental variables

Four important experimental variables, namely catalyst/*n*-caprylic acid molar ratio, methanol/*n*-caprylic acid ratio, reaction time, and temperature, were chosen for process optimization study during esterification reaction. The catalytic data obtained over the $[MIM\text{-}PSH]_{2.0}H_{2.0}PVMo_{11}O_{40}$ catalyst are displayed in Fig. 3. The methyl caprylate yield rose dramatically as the catalyst amount increased and achieved a maximum value when 0.52 mol% of catalyst to caprylic acid was added. As shown earlier, ultra-strong acidity may be unfavorable for the esterification reaction. This is most likely due to the occurrence of acid-catalyzed reverse reactions that, in turn, tend to spoil the product yield. As shown in Fig. 3a, when the catalyst to *n*-caprylic acid ratio exceeded 0.52 mol%, notable decrease in product yield was observed, most likely due to the hydrolysis of methyl caprylate to *n*-caprylic acid and methanol. The reason might be that more active moieties were available with the catalyst to *n*-caprylic acid molar ratio increasing. However, a slight decrease of the yield was observed when catalyst to *n*-caprylic acid molar ratio exceeded 0.52 mol%. This might be due to the side effect which derived from the acidity of excessive $[MIM\text{-}PSH]_{2.0}H_{2.0}PVMo_{11}O_{40}$ [44]. Taking into account the efficiency of catalyst and the issue of cost, the catalyst to *n*-caprylic acid molar ratio should be around 0.52 mol%.

Since esterification reaction was a reversible reaction, this made the amount of reactants play a crucial experimental parameter. As shown in Fig. 3b, the ester product (methyl caprylate) yield enhanced smoothly with increasing alcohol (methanol) to fatty (*n*-caprylic acid) ratio, reaching a maximum at a methanol/*n*-caprylic molar ratio of about 7.5, then, decline slowly thereafter. Thus, the esterification reason was favorable for excessive amount of alcohol than fatty acid, up

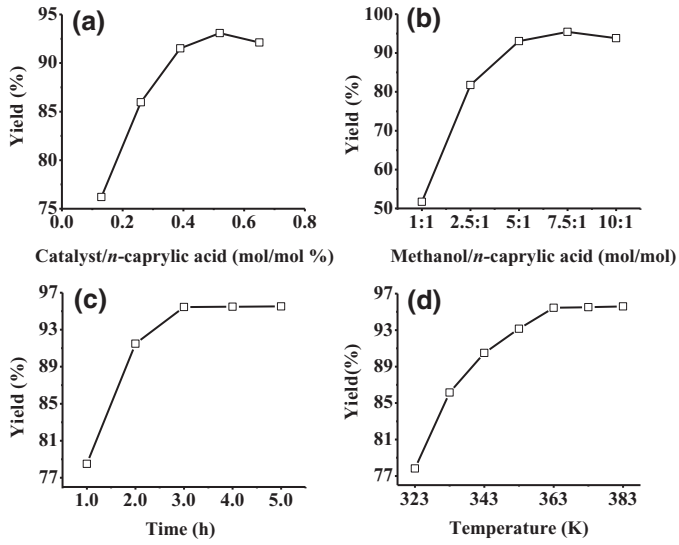

Fig. 3. Correlations of methyl caprylate yield with various experimental parameters: (a) catalyst to *n*-caprylic acid ratio, (b) methanol to *n*-caprylic acid ratio, (c) reaction time, and (d) temperature obtained during esterification of *n*-caprylic acid with methanol over the $[MIM\text{-}PSH]_{2.0}H_{2.0}PVMo_{11}O_{40}$ catalyst (see text). Note that while varying each experimental variable, other parameters were kept constant at their predicted values: catalyst to *n*-caprylic acid ratio = 0.52 mol%; methanol/*n*-caprylic acid ratio = 7.5, reaction time = 3.0 h, and temperature = 363 K.

Table 2
List of symbols and coded levels for corresponding experimental variables and ranges adopted during esterification reaction of *n*-caprylic acid with methanol over the $[MIM\text{-}PSH]_{2.0}H_{2.0}PVMo_{11}O_{40}$ catalyst.

Variable (unit)	Symbol	Range and level		
		−1	0	1
Catalyst/*n*-caprylic acid (mol/mol%)	x_1	0.39	0.52	0.65
Methanol/*n*-caprylic acid (mol/mol)	x_2	5.0	7.5	10
Reaction time (h)	x_3	2.5	3.0	3.5

to a maximum methanol/*n*-caprylic acid ratio of *ca.* 7.5 (*vide infra*). Further increasing this ratio (> 7.5) would only hamper the reaction since the residual methanol tended to dilute the reaction mixture, leading to an inferior reactivity, and hence, a lower methyl caprylate yield. Similar effect of alcohol/acid ratio on conversion was also observed for esterification of acids with alcohol over other acid catalysts [36,42,45].

The effect of reaction time on esterification activity was also examined. As shown in Fig. 3c, the product yield increased with increasing reaction time, then, reached a plateau at about 3.0 h. It is anticipated that, as the reaction reached its equilibrium, the esters produced may partially hydrolyzed to favor the reverse reaction. Thus, in view of the energy consumption, a desirable reaction time should be around 3.0 h. This observation is in good agreement with an earlier literature report [46]. Likewise, the influence of reaction temperature on esterification over the $[MIM\text{-}PSH]_{2.0}H_{2.0}PVMo_{11}O_{40}$ catalyst is shown in Fig. 3d. It was clear that the methyl caprylate yield increased notably as the reaction temperature increased from 323 to 363 K while continuously removing the produced water by methanol evaporation. However, no further change in ester yield was observed when the reaction temperature was raised above 363 K. This was due to the fact that methanol tended to evaporate more easily above its boiling point (337.8 K) [47].

3.4. Process optimization

The experimental variables listed in Table 2 were further optimized by the RSM method. The three experimental variables were designed at three levels coded with a plus sign (+1; high value), zero (0; central value), or a minus sign (−1; low value). Accordingly, the design of experiments and the predicted responses for the esterification catalyzed by the $[MIM\text{-}PSH]_{2.0}H_{2.0}PVMo_{11}O_{40}$ catalyst were summarized in Table 3 along with the experimental results. The methyl caprylate yield (*Y*) associated with various experimental variables and respective levels were predicted based on a quadratic model:

$$Y = 95.45 + 0.23x_1 - 0.39x_2 + 1.39x_3 - 0.93x_1^2 - 0.63x_2^2 - 1.70x_3^2 - 0.34x_1x_2 - 0.55x_1x_3 + 0.57x_2x_3 \quad (2)$$

where x_1, x_2 and x_3 were the coded values of the variables representing catalyst/*n*-caprylic acid molar ratio, methanol/*n*-caprylic acid molar ratio, and reaction time, respectively (*cf.* Table 2). The results clearly indicated that the predicted product yields were in close resemblance with the experimental values.

Table 3
List of experimental design and response values for esterification of *n*-caprylic acid with methanol.

Entry	Process variable and level			Methyl caprylate yield (%)	
	x_1	x_2	x_3	Experimental	Predicted
1	−1	−1	0	93.95	93.71
2	1	−1	0	94.73	94.85
3	−1	1	0	93.73	93.61
4	1	1	0	93.14	93.38
5	−1	0	−1	90.49	90.64
6	1	0	−1	92.40	92.20
7	−1	0	1	94.33	94.53
8	1	0	1	94.04	93.89
9	0	−1	−1	92.60	92.68
10	0	1	−1	90.80	90.76
11	0	−1	1	94.30	94.34
12	0	1	1	94.77	94.69
13	0	0	0	95.25	95.45
14	0	0	0	95.40	95.45
15	0	0	0	95.74	95.45
16	0	0	0	95.27	95.45
17	0	0	0	95.59	95.45

The fitting quality of the quadratic model in Eq. (2) was further verified by the standard analysis of variance (ANOVA). The results were depicted in Table 4. A much higher model *F*-value of 65.41 than its tabular counterpart ($F_{0.01,9,7} = 6.71$) was obtained, indicating that the model was highly significant. Meanwhile, the obtained *P*-value (< 0.0001) justified that the probability for such a large "model *F*-value" observed could occur due to noise is very slim (less than 0.01%). The obtained "Lack of fit *F*-value" of 2.16 also implies that it is insignificant relative to the pure error. As revealed by the obtained coefficient of determination ($R^2 = 0.9882$), the model was fairly reliable in predicting the responses, more than 98% of the experimental variables were covered. The obtained "Predicted *R*-square value" value of 0.8768 was also coincided with the "Adjusted *R*-squared value" (0.9731). The predicted R^2 was within 0.2 difference compared to the adjusted R^2 [48]. The "Adeq Precision" of 24.242, which measured the signal to noise ratio, was also much greater than the desirable value (4), indicating an adequate precision. Moreover, an observed coefficient of variation (C.V.) of 0.28% confirmed that the experiments were conducted reliably. As a result, the three independent variables as well as their mutual interactions were all highly significant to the esterification reaction.

Accordingly, the three dimensional (3D) response plots and contour plots obtained from the predicted model, which revealed correlations between two experimental variables (while keeping the other variable constant), were shown in Fig. S3 (Supplementary materials). As shown in Figs. S3a (Supplementary materials), the correlation between the catalyst to *n*-caprylic acid ratio (x_1) and methanol to *n*-caprylic acid ratio (x_2) clearly indicated the two variables were significant. At first, a gradual increased in methyl caprylate yield with

Table 4
Estimated regression coefficients and corresponding statistical *F*- and *P*-values for methyl caprylate yield.

Source	Sum of square	DF[a]	Mean square	*F*-value	*P*-value	Significance[b]
Model	39.32	9	4.37	65.41	< 0.0001	**
x_1	0.41	1	0.41	6.13	0.0424	*
x_2	1.23	1	1.23	18.45	0.0036	**
x_3	15.54	1	15.54	232.68	< 0.0001	**
x_1^2	3.66	1	3.66	54.82	0.0001	**
x_2^2	1.67	1	1.67	25.02	0.0016	**
x_3^2	12.20	1	12.20	182.73	< 0.0001	**
x_1x_2	0.47	1	0.47	7.03	0.0329	*
x_1x_3	1.21	1	1.21	18.12	0.0038	**
x_2x_3	1.29	1	1.29	19.29	0.0032	**
Residual	0.47	7	0.067			
Lack of fit	0.29	3	0.096	2.16	0.2358	
Pure error	0.18	4	0.045			
Cor total	39.79	16				

[a] DF denotes degree of freedom.
[b] * Represents significant; and ** represents highly significant.

increasing x_1 and x_2 was respectively observed, then slightly declined gradually upon further increasing the value of the variable. The contour plot (Fig. S3d; Supporting materials) further revealed that the interactions between these two variables was significant, in agreement with the ANOVA results (Table 4). Moreover, the correlations between the catalyst to *n*-caprylic acid ratio (x_1) and reaction time (x_3) over the methyl caprylate yield may be inferred from Fig. S3b and e (Supplementary materials). The ellipse mound shape of the contour line observed in Figs. S3b revealed that reaction time represented a more influential variable to the esterification process than catalyst to *n*-caprylic acid ratio, and the interactions between these two factors were fairly significant, which was consistent with the ANOVA results in Table 4. Likewise, the correlations between the methanol to *n*-caprylic acid ratio (x_2) and reaction time (x_3) towards the esterification reaction may be seen from Fig. S3c and f (Supplementary material). The tilted ellipse response curve (Fig. S3c) showed that reaction time had more significant impact on the product yield than the alcohol to acid ratio and the interactions between two variables were also significant to the esterification reaction over the [MIM-PSH]$_{2.0}$H$_{2.0}$PVMo$_{11}$O$_{40}$ catalyst, as expected (*cf.* Table 4).

Based on the RSM studies and Eq. (2), an optimum methyl caprylate yield of 95.74% may be predicted for the esterification over the [MIM-PSH]$_{2.0}$H$_{2.0}$PVMo$_{11}$O$_{40}$ catalyst under the conditions: x_1 (catalyst to *n*-caprylic acid ratio) = 0.52 mol%, x_2 (methanol to *n*-caprylic acid ratio) = 7.12, and x_3 (reaction time) = 3.19 h at a reaction temperature of 363 K (*cf.*, Table 2). These optimized variables and validity of the mathematical model were tested by additional experimental studies, however, the following approximate values were adopted for matter of convenience: x_1 = 0.52 mol%, x_2 = 7, x_3 = 3 h, and temperature 363 K. To afford a more accurate experimental result, three parallel experiments were carried out under the above modified conditions. As a result, an average experimental methyl caprylate yield of 95.6% was obtained, which was in excellent agreement with the predicted value. This indicated that the proposed model was reliable and the regression equation truly reflected the influence of three independent variables on the product yield of the esterification reaction.

3.5. Catalyst recyclability

Finally, to assess the recyclability of the catalyst, which was a crucial factor for practical industrial applications, additional cyclic studies were conducted. The cyclic experiments were carried out under the aforementioned optimal operation conditions over the [MIM-PSH]$_{2.0}$H$_{2.0}$PVMo$_{11}$O$_{40}$ catalyst. Upon completion of the reaction for each cycle, the lower layer of the reaction mixture (which formed automatically due to self-separation characteristic of the system) was collected by filtration, followed by repeated washing diethyl ether, and dried under vacuum for 5.0 h at 343 K. The catalyst so extracted by such simple procedure was then reused for the next experimental run. The collective results were depicted in Fig. 4, which revealed no remarkable loss in catalytic activity over six consecutive runs, implying an excellent durability and recyclability of the novel heteropolyacid-based ionic liquid catalyst.

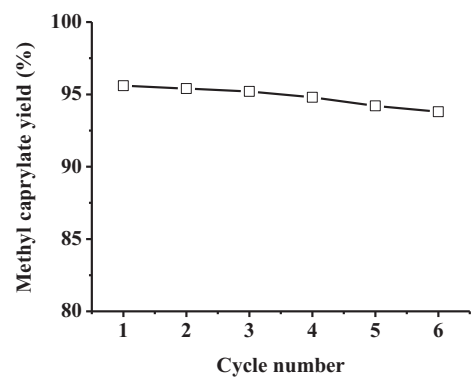

Fig. 4. Stability of the [MIM-PSH]$_{2.0}$H$_{2.0}$PVMo$_{11}$O$_{40}$ catalyst during esterification of *n*-caprylic acid with methanol. Reaction conditions: catalyst/*n*-caprylic acid = 0.52 mol%, methanol/*n*-caprylic acid = 7, time = 3 h, and temperature = 363 K.

4. Conclusions

In summary, a series of novel heteropolyacid (HPA)-based ionic liquid (IL) catalysts, namely [MIM-PSH]$_x$H$_{4-x}$PVMo$_{11}$O$_{40}$ (x = 0.0–4.0), have been successfully synthesized and applied for esterification of *n*-caprylic acid with methanol. Among various catalysts examined, the [MIM-PSH]$_{2.0}$H$_{2.0}$PVMo$_{11}$O$_{40}$ sample exhibited the optimum catalytic performance for esterification of *n*-caprylic acid to methyl caprylate. The effects of process variables on esterification over the [MIM-PSH]$_{2.0}$H$_{2.0}$PVMo$_{11}$O$_{40}$ catalyst were investigated and relevant optimal operating conditions deduced form process optimization using the response surface methodology (RSM) were: catalyst to *n*-caprylic acid molar ratio (x_1) = 0.52 mol%, methanol to *n*-caprylic acid molar ratio (x_2) = 7.12, and reaction time (x_3) = 3.19 h while at a reaction temperature of 363 K. Consequently, an experimental methyl caprylate yield of 95.6% was obtained under modified experimental variables of x_1 = 0.52 mol%, x_2 = 7, and x_3 = 3 h at 363 K, which was in excellent agreement with the predicted yield of 95.74%. Such HPA-IL composite catalysts which can be synthesized

by a facile method also possess unique self-separation properties and durabilities that are favorable for product separation and catalyst recycle show prospective industrial applications as practical catalysts for conversion of biomass to valuable chemicals and biodiesels.

Acknowledgments

The supports of this work by the National Natural Science Foundation of China (No. 21177110), the National Natural Science Foundation of Zhejiang Province, China (No. LY13B070005), the Program for Zhejiang Leading Team of S & T Innovation (No. 2013TD07), and the Ministry of Science and Technology, Taiwan (NSC101-2113-M-001-020-MY3) are gratefully acknowledged.

Supplementary materials

Supplementary material associated with this article can be found, in the online version, at doi:10.1016/j.jtice.2015.07.005.

References

[1] Otera J. Esterification: methods, reactions, and applications. 1st ed. Wiley-VCH; 2003.
[2] Liu Y, Lotero E, Goodwin Jr JG. Effect of water on sulfuric acid catalyzed esterification. J Mol Catal A 2006;245:132–40.
[3] Aafaqi R, Mohamed AR, Bhatia S. Kinetics of esterification of palmitic acid with isopropanol using p-toluene sulfonic acid and zinc ethanoate supported over silica gel as catalysts. J Chem Technol Biotechnol 2004;79:1127–34.
[4] Kang Q, Zhao ZA, You SL. Highly enantioselective Friedel–Crafts reaction of indoles with imines by a chiral phosphoric acid. J Am Chem Soc 2007;129:1484–5.
[5] Mizuno N, Misono M. Heterogeneous catalysis. Chem Rev 1998;98:199–217.
[6] Kiakalaieh AT, Amin NAS, Zarei A, Noshadi I. Transesterification of waste cooking oil by heteropolyacid (HPA) catalyst: optimization and kinetic model. Appl Energy 2013;102:283–92.
[7] Karimi B, Vafaeezadeh M. SBA-15-functionalized sulfonic acid confined acidic ionic liquid: a powerful and water-tolerant catalyst for solvent-free esterifications. Chem Commun 2012;48:3327–9.
[8] Sakthivel A, Komura K, Sugi Y. MCM-48 supported tungstophosphoric acid: an efficient catalyst for the esterification of long-chain fatty acids and alcohols in supercritical carbon dioxide. Ind Eng Chem Res 2008;47:2538–44.
[9] Saravanan K, Tyagi B, Bajaj HC. Esterification of caprylic acid with alcohol over nano-crystalline sulfated zirconia. J Sol-Gel Sci Technol 2012;62:13–17.
[10] Chung KH, Park BG. Esterification of oleic acid in soybean oil on zeolite catalysts with different acidity. J Ind Eng Chem 2009;15:388–92.
[11] Patel D, Saha B. Esterification of acetic acid with *n*-hexanol in batch and continuous chromatographic reactors using a gelular ion-exchange resin as a catalyst. Ind Eng Chem Res 2012;51:11965–74.
[12] Huang W, Xia YM, Gao H, Fang YJ, Wang Y, Fang Y. Enzymatic esterification between *n*-alcohol homologs and *n*-caprylic acid in non-aqueous medium under microwave irradiation. J Mol Catal B 2005;35:113–16.
[13] Zhao Z, Li Z, Wang G, Qiao W, Cheng L. Heteropolyacids catalysts and their application in the synthesis of fine chemicals. Prog Chem 2004;16:620–30 (In Chinese).
[14] Obali Z, Dogu T. Activated carbon-tungstophosphoric acid catalysts for the synthesis of *tert*-amyl ethyl ethe (TAEE). Chem Eng J 2008;138:548–55.
[15] Bhatt N, Patel A. Supported 12-tungstophosphoricacid: a recoverable solid acid catalyst for liquid phase Friedel–Crafts alkylation of phenol. J Taiwan Inst Chem E 2011;42:356–62.
[16] Srilatha K, Ramesh Kumar C, Prabhavathi Devi BLA. Efficient solid acid catalysts for esterification of free fatty acids with methanol for the production of biodiesel. Catal Sci Technol 2011;1:662–8.
[17] Sunita G, Devassy BM, Vinu A, Sawant DP, Balasubramanian VV, Halligudi SB. Synthesis of biodiesel over zirconia-supported isopoly and heteropoly tungstate catalysts. Catal Commun 2008;9:696–702.
[18] Moosavifar M. An appropriate one-pot synthesis of dihydropyrimidinones catalyzed by heteropolyacid supported on zeolite: an efficient and reusable catalyst for the Biginelli reaction. C R Chim 2012;15:444–7.
[19] Engin A, Haluk H, Gurkan K. Production of lactic acid esters catalyzed by heteropolyacid supported over ion-exchange resins. Green Chem 2003;5:460–6.
[20] Bhorodwaj SK, Dutta DK. Heteropolyacid supported modified montmorillonite clay: an effective catalyst for the esterification of acetic acid with *sec*-butanol. Appl Catal A 2010;378:221–6.
[21] Hagiwara R, Ito Y. Room temperature ionic liquids of alkylimidazolium cations and fluoroanions. J Fluor Chem 2000;105:221–7.
[22] Welton T. Room-temperature ionic liquids. Solvents for synthesis and catalysis.. Chem Rev 1999;99:2071–83.
[23] Zhao D, Ge J, Zhai J, Zhang J, Liu M, Li J. Synthesis of succinic acid diisopropyl ester catalyzed by Lewis acidic ionic liquids. J Chem Ind Eng 2014;2:561–9 (In Chinese).
[24] Wang E, Gao L, Liu J, Liu Z, Yan D. Preparation and properties of the molybdovanadophosphoric acid with Dawson Structure. Acta Chim Sin 1988;46:757–62.
[25] Du H, He Y, Tan Z, Han X. Catalytic synthesis of butyl isovalerate by Brønsted acidic ionic liquid under microwave irradiation. Asian J Chem 2013;25:7675–8.
[26] Zhao Q, Chen WH, Huang SJ, Wu YC, Lee HK, Liu SB. Discernment and quantification of internal and external acid sites on zeolites. J Phys Chem B 2002;106:4462–9.
[27] Zheng A, Huang SJ, Liu SB, Deng F. Acid properties of solid acid catalysts characterized by solid-state ^{31}P NMR of adsorbed phosphorous probe molecules. Phys Chem Chem Phys 2011;13:14889–901.
[28] Zheng A, Deng F, Liu SB. Acidity characterization of solid acid catalysts by solid-state ^{31}P NMR of adsorbed phosphorus-containing probe molecules. Annu Rep NMR Spectrosc 2014;81:47–108.
[29] Han X, He Y, Hung CT, Liu LL, Huang SJ, Liu SB. Efficient and reusable polyoxometalate-based sulfonated ionic liquid catalysts for palmitic acid esterification to biodiesel. Chem Eng Sci 2013;104:64–72.
[30] Khuri AI, Cornell JA. Response surfaces: designs and analyses. New York, NY: Marcel Dekker; 1987.
[31] Rao PM, Wolfson A, Kababya S, Vega S, Landau MV. Immobilization of molecular $H_3PW_{12}O_{40}$ heteropolyacid catalyst in alumina-grafted silica-gel and mesostructured SBA-15 silica matrices. J Catal 2005;232:210–25.
[32] Karimi B, Elhamifar D, Yari O, Khorasani M, Vali H, Clark JH, Hunt AJ. Synthesis and characterization of alkyl-imidazolium-based periodic mesoporous organosilicas: a versatile host for the immobilization of perruthenate (RuO^{4-}) in the aerobic oxidation of alcohols. Chem Eur J 2012;18:13520–30.
[33] Bordoloi A, Sahoo S, Lefebvre F, Halligudi SB. Heteropolyacid-based supported ionic liquid-phase catalyst for the selective oxidation of alcohols. J Catal 2008;259:232–9.
[34] Deng WJ, Zhu WS, Xiong J, Yang L, Wei AM, Zhang M, Li HM. Novel heterogeneous iron-based redox ionic liquid supported on SBA-15 for deep oxidative desulfurization of fuels. Chem Eng J 2015;266:213–21.
[35] Jing L, Zhang FM, Zhong YJ, Zhu WD. Hydroxylation of benzene to phenol by H_2O_2 over an inorganic–organic dual modified heteropolyacid. Chin J Chem Eng 2014;22:1220–5.
[36] Han X, Yan W, Chen K, Hung CT, Liu LL, Wu PH, Huang SJ, Liu SB. Heteropolyacid-based ionic liquids as effective catalysts for the synthesis of benzaldehyde glycol acetal. Appl Catal A 2014;485:149–56.
[37] Han X, Du H, Hung CT, Liu LL, Wu PH, Ren D, Huang SJ, Liu SB. Syntheses of novel halogen-free Brønsted–Lewis acidic ionic liquid catalysts and their applications for synthesis of methyl caprylate. Green Chem 2015;17:499–508.
[38] Zheng A, Zhang H, Lu X, Liu SB, Deng F. Theoretical predictions of ^{31}P NMR chemical shift threshold of trimethylphosphine oxide absorbed on solid acid catalysts. J Phys Chem B 2008;112:4496–505.
[39] Zheng A, Huang SJ, Chen WH, Wu PH, Zhang H, Lee HK, de Menorval LC, Deng F, Liu SB. ^{31}P Chemical shift of adsorbed trialkylphosphine oxides for acidity characterization of solid acids catalysts. J Phys Chem A 2008;112:7349–56.
[40] Feng N, Zheng A, Huang SJ, Zhang H, Yu N, Yang CY, Liu SB, Deng F. Combined solid-state NMR and theoretical calculation studies of Brønsted acid properties in anhydrous 12-molybdophosphoric acid. J Phys Chem C 2010;114:15464–72.
[41] Huang SJ, Yang CY, Zheng A, Feng N, Yu N, Wu PH, Chang YC, Lin YC, Deng F, Liu SB. New insights of Keggin-type 12-tungstophosphoric acid from ^{31}P MAS NMR of adsorbed trimethylphosphine oxide and DFT calculation studies. Chem-Asian J 2011;6:137–48.
[42] Leng Y, Wang J, Zhu DR, Wu YJ, Zhao PP. Sulfonated organic heteropolyacid salts: recyclable green solid catalysts for esterifications. J Mol Catal A 2009;313:1–6.
[43] Huang MY, Han X, Hung CT, Lin JC, Wu PH, Wu JC, Liu SB. Heteropolyacid-based ionic liquids as efficient homogeneous catalysts for acetylation of glycerol. J Catal 2014;320:42–51.
[44] Li RJ, Chen L, Yan ZC. Synthesis of trimethylolpropane esters of oleic acid using a multi-SO_3H-functionalized ionic liquid as an efficient catalyst. J Am Oil Chem Soc 2012;89:705–11.
[45] Zhang L, Xian M, He YC, Li LZ, Yu ST, Xu X. A Brønsted acidic ionic liquid as an efficient and environmentally benign catalyst for biodiesel synthesis from free fatty acids and alcohols. Bioresour Technol 2009;100:4368–73.
[46] Aghabarari B, dorostkar N, Ghiaci M, Amini SG, Rahimi E, Martinez-Huerta MV. Esterification of fatty acids by new ionic liquids as acid catalysts. J Taiwan Inst Chem E 2014;45:431–5.
[47] Saravanan K, Tyagi B, Shukla SR, Bajaj HC. Esterification of palmitic acid with methanol over template-assisted mesoporous sulfated zirconia solid acid catalyst. Appl Catal B 2015;172–173:108–15.
[48] Hosseinpour V, Kazemeini M, Mohammadrezaee A. A study of the water–gas shift reaction in Ru-promoted Ir-catalysed methanol carbonylation utilising experimental design methodology. Chem Eng Sci 2011;66:4798–806.